C-glyco"RGD" as αIIbβ3 and αvβ integrin ligands for imaging applications: synthesis, in vitro evaluation and molecular modeling

Timothé Vucko, Nicolas Pétry, François Dehez, Alexandrine Lambert, Antonio Monari, Cécile Lakomy, Patrick Lacolley, Véronique Regnault, Charlotte Collet, Gilles Karcher, et al.

Bioorganic & Medicinal Chemistry
journal homepage: www.elsevier.com

C-glyco"RGD" as $\alpha_{IIb}\beta_3$ and $\alpha_v\beta$ integrin ligands for imaging applications: synthesis, in vitro evaluation and molecular modeling.

Timothé Vucko[a], Nicolas Pétry[a,#], François Dehez[b], Alexandrine Lambert[b], Antonio Monari[b], Cécile Lakomy[c], Patrick Lacolley[c], Véronique Regnault[c], Charlotte Collet[d,e], Gilles Karcher[d], Nadia Pellegrini-Moïse[a], Sandrine Lamandé-Langle[a,*]

[a] *Université de Lorraine, CNRS, L2CM, F-5400 Nancy, France*
[b] *Université de Lorraine, CNRS, LPCT, F-54000 Nancy, France*
[c] *Université de Lorraine, Inserm, DCAC, F-54500 Nancy, France*
[d] *NancycloTEP, Plateforme d'imagerie moléculaire, F-54511 Vandoeuvre-lès-Nancy, France*
[e] *Université de Lorraine, INSERM, U1254 IADI, F-54000 Nancy, France*
[#] *Present address: Institut des Biomolécules Max Mousseron (IBMM), UMR 5247, UM, CNRS, ENSCM, Université de Montpellier Campus Triolet Place Eugène Bataillon, 34095 Montpellier cedex 5, France.*

ARTICLE INFO

Article history:
Received
Received in revised form
Accepted
Available online

Keywords:
Glycopeptide
RGD
C-glycoside
Integrins

ABSTRACT

The design of conjugates displaying simultaneously high selectivity and high affinity for different subtypes of integrins is a current challenge. The arginine-glycine-aspartic acid amino acid sequence (RGD) is one of the most efficient short peptides targeting these receptors. We report herein the development of linear and cyclic fluoro-*C*-glycoside"RGD" conjugates, taking advantage of the robustness and hydrophilicity of *C*-glycosides. As attested by *in vitro* evaluation, the design of these *C*-glyco"RGD" with a flexible three-carbon triazolyl linker allows distinct profiles towards $\alpha_{IIb}\beta_3$ and $\alpha_v\beta_3$ integrins. Molecular-dynamics simulations confirm the suitability of cyclic *C*-glyco-c(RGDfC) to target $\alpha_v\beta_3$ integrin. These *C*-glyco"RGD" could become promising biological tools in particular for Positron Emission Tomography imaging.

1. Introduction

Angiogenesis is a fundamental process involved in tumor growth, malignant transformation of tumors and metastasis.[1,2,3] Integrins are heterodimeric cell-adhesion proteins involved in angiogenesis signaling pathways and overexpressed in many angiogenic processes. These receptors mediate the attachment of cells to the extracellular matrix and are crucial for cell-to-cell interactions.[4-6] Integrins are composed of two non-covalently associated subunits: an α domain and a β domain, whose combination determines signaling properties and ligand binding affinity.[4,6,7] During angiogenesis, αv integrins are overexpressed on the surface of endothelial cells in angiogenic vessels to promote their growth and survival. The most extensively studied integrin is the $\alpha_v\beta_3$ integrin, which represents a highly specific biomarker, in particular to monitor tumor progression.[8-10] The $\alpha_{IIb}\beta_3$ integrin lying across the plasma membrane of human platelets is also widely studied. Its physiological function is intimately linked to the process of platelet activation and thrombosis.[6,11,12] Therefore, both integrins represent valuable targets for diagnostic and therapeutic approaches.

Because of its ability to bind integrins, the arginine-glycine-aspartic acid amino acid sequence (RGD) is one of the most studied short peptides.[13,14] Linear RGD sequences were first explored but showed low affinities and degradation in biological environments.[13,15] Cyclic RGD peptides, such as c(RGDfK) or c(RGDyC), containing a conformationally constrained RGD sequence, exhibit enhanced *in vivo* stability and improved binding to some integrins.[10,15,16] RGD labeled probes have been extensively used in cancer research ($\alpha_v\beta_3$)[8,16-18] but also widely applied in platelet biology for thrombosis imaging ($\alpha_{IIb}\beta_3$).[12,16,18-20] These RGD labeled probes employed for biophysical and medical applications, including molecular imaging (e. g. Positron Emission Tomography (PET)), were prepared by introducing a functional unit capable of binding covalently an opportune dye. By using an appropriate anchoring point in the peptide sequence, the loss of activity induced by the functionalization could be minimized. For

* *Corresponding author. Tel.: +33 372745585; e-mail:* sandrine.langle@univ-lorraine.fr

instance, c(RGDfK) and c(RGDfC) cyclopeptides are often used as both lysine and cysteine lateral chains are efficient anchors while such modifications do not generally significantly affect the binding affinity of the native peptide.[16]

The inherent physico-chemical properties of peptides impair their biodistribution,[21] limiting their direct use in the cellular context. The introduction of a carbohydrate moiety on bioactive peptides has been shown to reduce significantly their lipophilicity and consequently enhancing their bioavailability, pharmacokinetics, and *in vivo* clearance properties, which is of great interest for therapeutic and diagnostic applications.[22,23] Moreover, it has been demonstrated that the inclusion of a carbohydrate moiety enhances the capacity of the conjugate peptide to form intermolecular interactions, inducing enriched functionalities such as the ability to modulate peptide structure and cell–cell recognition in multicellular systems.[24,25] Notably, the glycosylation of RGD containing peptides has proven useful in particular to target tumor cells and for imaging of tumor angiogenesis.[23,26-33]

The applicability of cyclic RGD-glycoconjugates in PET imaging has been recently investigated. Prante and coworkers synthetized glyco"RGD" by forming either a C-N or a C-S bond directly on the pseudo-anomeric center.[27,31,33] Haubner's group developed c(RGDfK) conjugated on position 6 of a sugar amino acid.[23,28,29] We prepared glyco"RGD" where an *O*-glycosidic moiety was grafted on the RGD peptide by means of a spacer arm.[19,34-36]

In the perspective of developing more performant and selective diagnostic tools for PET imaging, the use of RGD derivatives conjugated with a *C*-glycosidic moiety appears as an appealing strategy. Some *O*-glycoside RGD derivatives previously developed[19,34] are recognized by glycosidases, eventually hydrolyzing their *O*-glycosidic bond and limiting thereby their stability in vivo. Interestingly, *C*-glycosyl compounds, which is a subject of interest in our group for several years,[37-40] are resistant to acidic and enzymatic hydrolysis thanks to their robust C-C link in anomeric position, conferring them a high in vivo stability.[41,42] Copper-catalyzed azide-alkyne cycloaddition (CuAAC) is an ideal tool for conjugating a sugar moiety to RGD peptides.[34,43,44] It produces a stable triazolyl group which could further increase the peptide binding affinity for integrins.[32,45]

In this contribution, we designed a new type of glyco"RGD" integrating a stable and flexible *C*-glycosidic bond (Fig 1). A $^{19/18}$F-fluorine atom was introduced on the sugar moiety, allowing the future use of these glycosidic compounds as diagnostic tools for PET imaging. Cyclic and linear glyco"RGD" derivatives were synthetized and their ability to target integrins was evaluated *in vitro*. The experimental results were supplemented by molecular-dynamics simulations, offering an atomistic description of the binding patterns of *C*-glyco"RGD" and $\alpha_v\beta_3$ integrin.

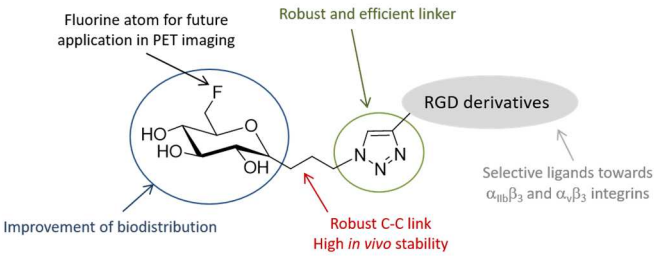

Fig 1. Schematic topology of *C*-glyco"RGD" compounds.

2. Results

2.1. Synthesis of C-glyco"RGD".

The synthesis of new *C*-glyco"RGD" derivatives by CuAAC requires that one partner bears an azido group and the other a propargyl function. Based on our expertise in the synthesis of *O*-glycopeptides by CuAAC,[19,35,36] we introduced propargyl and azide moieties on peptide and sugar groups respectively. Indeed, propargyl bromide is easily and quickly introduced on the thiol group of cysteine-containing peptides by a standard alkylation reaction in aqueous medium.[19,35,46] *C*-glycosides containing an azido propyl arm on the anomeric carbon were chosen as sugar derivative to take advantage of the flexibility given by the three carbons arm between the carbohydrate and the triazole of the final *C*-glyco"RGD" conjugate. In this study, we focused on a glucopyranose in both α and β configurations after introduction of the flexible arm (Scheme 1).

Bromo derivatives **2** (β configuration) and **3** (α configuration) were prepared according to known methods[47] (Scheme 1). Briefly, 1-*O*-acetyl-2,3,4,6-tetra-*O*-benzyl-D-glucopyranose **1**[48,49] was stereoselectively converted in the corresponding β- or α-*C*-allylglucopyranoside.[50-53] The alkenes were treated with 9-Borabicyclo(3.3.1)nonane (9-BBN)[54,47] and the resulting alcohols were converted in bromide derivatives **2** and **3**.[47] Analogous pathways were then carried out on both anomers to provide the targeted azidopropyl-*C*-glycosides **14** and **15** (Scheme 1). The removal of the benzyl ether protecting groups by hydrogenolysis re-quired a meticulous optimization due to the presence of a bromide atom. We observed previously that catalytic hydrogenolysis under H_2 atmosphere (33 psi) with $Pd(OH)_2/C$ (20% w/w) in a THF/H_2O (5/1 v/v) mixture during 13 hours gave the best results for both β and α anomers.[55] The fully deprotected derivatives **4** and **5** were thus obtained in 95 and 93% yields respectively while the formation of debrominated side-product was limited. Compounds **4** and **5** were reacted with sodium azide in an acetone/water (5/1 v/v) mixture at reflux during 12 hours affording compounds **6** and **7**.[56] In a one-pot procedure, selective protection of the primary alcohol of **6** and **7** with a trityl group using trityl chloride and a catalytic amount of 4-dimethylaminopyridine (DMAP) followed by peracetylation produced intermediates **8** and **9** in 62 and 75% yields respectively. Compounds **10** and **11** were obtained after selective deprotection of the primary hydroxyl with trifluoroacetic acid (TFA) in dichloromethane at 0°C during 10 minutes in 73 and 75% yields respectively.[57]

In view of potential PET applications,[44,58] *C*-glycosyl derivatives were fluorinated at position 9 (numbering in Scheme 1) standing as a non-radioactive reference of prosthetic groups to be coupled to peptides. Indeed, in the perspective of fluorine-18 labeling, this position is the most reactive and ideally suited for introducing a fluorine atom via nucleophilic substitution. The reaction was carried out with (diethylamino)sulfur trifluoride (DAST) as a fluorinating agent in diglyme at 110°C to provide the corresponding 6-fluoro-*C*-glycosides **12** and **13**. ^{19}F-NMR of fluoro-compounds showed only one doublet of triplet, corresponding to the fluorine atom coupling with H9 and H8, observed around -231.4 ± 0.2 ppm with coupling constants around 47 and 21 Hz ($J_{F,H9}$ and $J_{F,H8}$ respectively). Zemplén deprotection (Na^0, MeOH) was then carried out leading to **14** (β-anomer) and **15** (α-anomer) in quantitative yields.

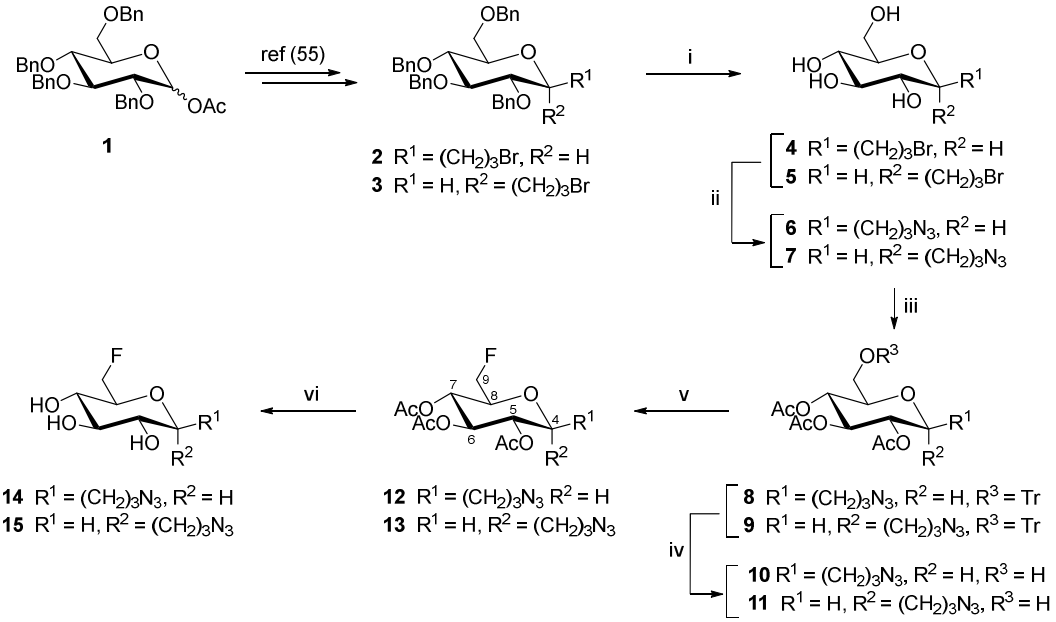

Scheme 1. 6-fluoro-C-glycosides synthesis. Reagents and conditions: (i) $Pd(OH)_2/C$ (20% w/w), THF/H_2O (5/1 v/v), H_2, 33 psi, 13h, **4** (95%) , **5** (93%); (ii) NaN_3, acetone/water (5/1 v/v), reflux, 12h, **6** (95%), **7** (96%); (iii) 1) TrCl, DMAP, pyridine, 48h, 45°C. 2) Ac_2O, 0°C to rt, 2h, **8** (62%), **9** (75%); (iv) TFA (20% v) in CH_2Cl_2, 0°C, 10 min, **10** (73%), **11** (75%); (v) DAST, diglyme, 110°C, 8 min, **12** (61%), **13** (52%); (vi) Na^0, MeOH, 25°C, 1h, quantitative.

Next, we introduced a triple bond on peptide derivatives. The S-propargylation of cysteine-containing RGD peptides was carried out by taking advantage of the high nucleophilicity of the thiol group of the cysteine. It has already been demonstrated that this simple, efficient and robust method[19,35,46] enables one-step propargylation of non-protected peptides. Two commercially available RGD peptides containing a cysteine residue were investigated, one linear tetrapeptide i.e. RGDC **16** and one cyclic pentapeptide i.e. c(RGDfC) **17**. Regioselective S-propargylation of the cysteine residue was carried out according to a described method,[19,35,46] giving the S-propargyl-RGD derivatives **18** and **19** in 85 and 82% yields respectively (Scheme 2).

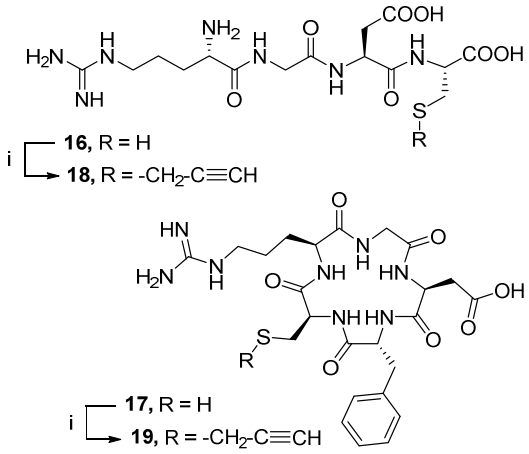

Scheme 2. Propargylation of RGD peptides. Reagents and conditions: (i) propargyl bromide (1.1 eq.), NH_4OH, H_2O, MeOH, 25°C, 3h, **18** (85%), **19** (82%).

Coupling of S-propargylated peptides **18** and **19** with 6-fluoro-*C*-glycosides **14** and **15** was performed via CuAAC. This rapid and usually side-product-free reaction proceeded efficiently under very mild conditions in water using copper (II) acetate (10 mol%) and sodium ascorbate (20 mol%) as reducing agent (Scheme 3).[19] Interestingly, the reaction medium turned pale green upon addition of copper acetate to the azide and alkyne mixture and became blue within 2 hours. TLC monitoring showed no unreacted *C*-glycoside and completion of the reaction. The workup consisted of removal of copper ions with a chelating resin (Chelex®) followed by freeze-drying. Linear and cyclic *C*-glyco"RGD" derivatives **20**-**23** were obtained in good yields (65-74%) after purification by steric exclusion gel filtration. As expected with these experimental conditions, the cycloaddition was regioselective and afforded 1,4-disubstituted-2,3,4-triazole as the only product in all cases (Scheme 3). High resolution mass spectrometry and 1D and 2D NMR data confirmed the structure of the cycloadducts.

S-propargyl-cysteine RGD derivatives reacted efficiently with azido-fluoro-C-glycosides in CuAAC click coupling whatever the anomeric configuration and the peptide type i.e. linear or cyclic. The reaction proceeds well in water in short reaction time. Beyond CuAAC advantages (*vide supra*), the incorporation of a triazole moiety in a peptide or glycopeptide is of particular interest in terms of electronic properties and potential additional (intra)molecular interactions.[32,45]

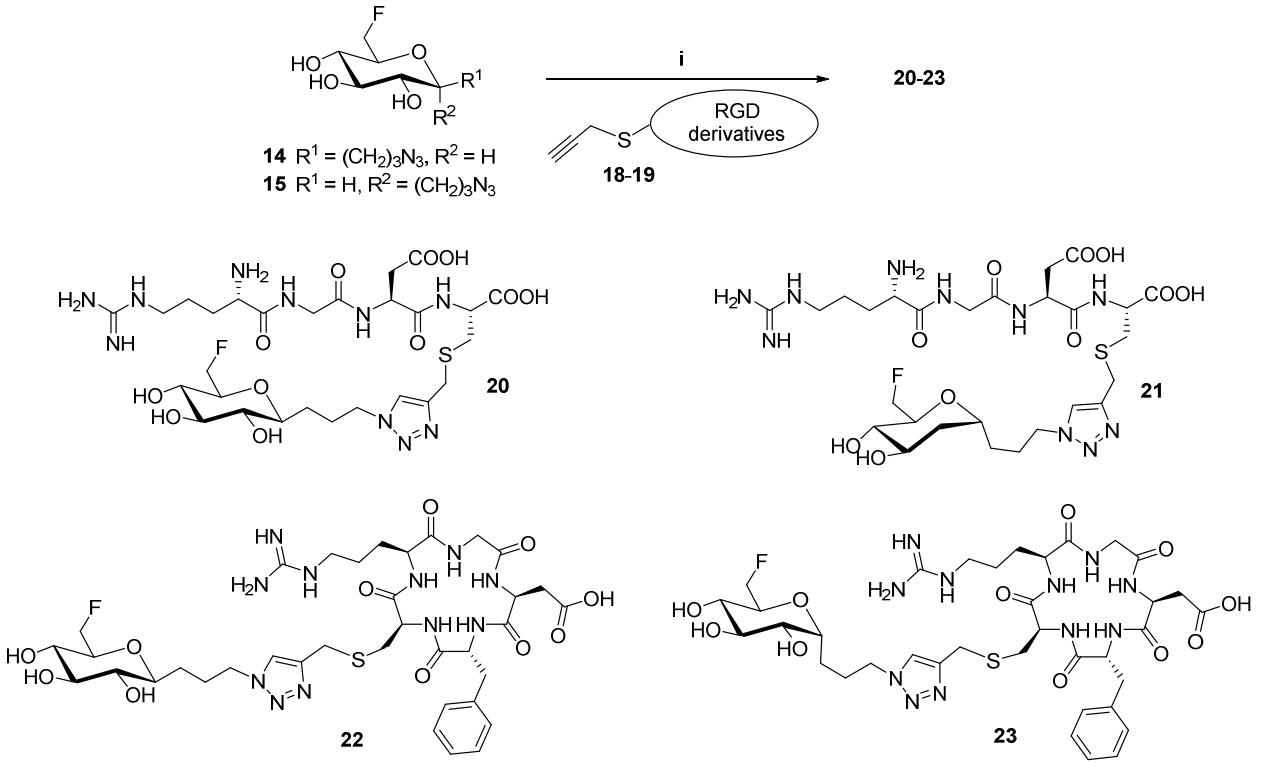

Scheme 3. Synthesis of *C*-glyco"RGD" derivatives **20**-**23**. Reagents and conditions: (i) H_2O, $Cu(OAc)_2$, Na Ascorbate, 25°C, 2h, **20** (74%), **21** (71%), **22** (69%), **23** (65%).

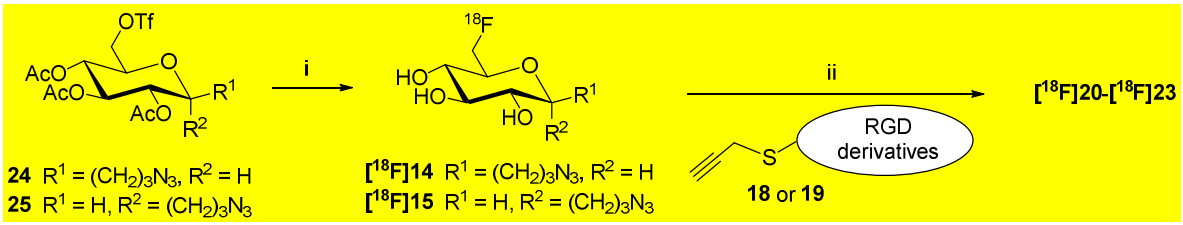

Scheme 4. Radiosynthesis of [^{18}F]F-*C*-glyco"RGD" derivatives **[^{18}F]20-[^{18}F]23**. Reagents and conditions: (i) 1) K[^{18}F]F-K_{222}, CH_3CN, 95°C, 5 min, decay-corrected radiochemical yields (48 to 69%). 2) HPLC purification. 3) NaOH, 30 °C, 9 min then HCl. (ii) $Cu(OAc)_2$, Na ascorbate, H_2O, 55°C, 25 min, (40 to 65 %).

^{18}F-radiosynthesis of [^{18}F]F-*C*-glyco"RGD" **[^{18}F]20-[^{18}F]23** was then investigated (Scheme 4). Precursors of radiolabeling **24** and **25** were easily obtained starting from **10** or **11** by reacting triflic anhydride with pyridine in 80% and 45% yield respectively. ^{18}F-radiolabeling of **24** and **25** was carried out on an AllInOne (AIO) synthesizer with classical method of radiofluorination using the K[^{18}F]F-K_{222} complex in acetonitrile at 95°C during 5 minutes. Radiolabelled mixture was then purified on a silica SPE cartridge following by semi-preparative HPLC. **[^{18}F]14** or **[^{18}F]15** was obtained after saponification with NaOH 1M of the collected product. After neutralization by HCl 1M, the CuAAC coupling was then implemented to afford **[^{18}F]20-[^{18}F]23**. The reaction proceeded with propargylated peptide (**18** or **19**), $Cu(OAc)_2$ and sodium ascorbate in water at 55°C during 25 min**.** Pre-purification of ^{18}F-labeled *C*-glyco"RGD" can be operated by simple filtration on a cartridge loaded with Chelex® 100 resin to remove most of the unreacted prosthetic group and copper. Semi-preparative HPLC of [^{18}F]F-*C*-glyco"RGD" was then performed. Identity of **[^{18}F]20-[^{18}F]23** was confirmed with analytical HPLC by a second injection with the authentic non-radioactive standard (identical t_R). **[^{18}F]20-[^{18}F]23** were radiosynthesized with satisfactory decay corrected radiochemical yields (2-4%) considering the complexity of the radiosynthesis.

2.2. In vitro evaluation.

The *in vitro* biological properties of the new linear and cyclic *C*-glyco"RGD" derivatives were evaluated on human platelets and human vascular smooth muscle cells (VSMCs) selected for their expression of $\alpha_{IIb}\beta_3$ and $\alpha_v\beta_3$ respectively.[8,12,16-20] Additionally, to assess the influence of the saccharide moiety, the biological effects of the corresponding reference peptides, i.e. RGDC and c(RGDfC), were also measured.

The ability of the four RGD-conjugates **20**-**23** to inhibit ADP-induced platelet aggregation was first evaluated. Platelet aggregation was triggered by 2.5 µM ADP in human citrated platelet-rich plasma (PRP adjusted to 300×109 platelets/L) after performing or not a preincubation with reference peptides RGDC **16**, c(RGDfC) **17** and *C*-glyco"RGD" **20**-**23** at concentrations varying from 12.5 to 200 µM (Fig 2). All peptides dose-dependently inhibited aggregation of PRP induced by 2.5 µM ADP. For all tested concentrations, linear *C*-glyco-RGDC **20** and **21** exerted a more potent inhibitory effect than RGDC and c(RGDfC) reference peptides whereas cyclic *C*-glyco-c(RGDfC) **22** and **23** had only a slight effect. IC_{50} values are listed in Table 1. As described in the literature,[16] the IC_{50} value was higher for the linear RGDC than for the cyclic c(RGDfC) reference peptides (compare entries 1 and 2). This is however not the case for the *C*-glyco"RGD" conjugates. Indeed, it appears that linear *C*-glyco-RGDC **20** and **21** are more effective inhibitors (IC_{50} of 100 and 65 µM respectively, entries 3 and 4) compared to both RGD

references (IC_{50} 223 and 139 µM). Conversely, cyclic *C*-glyco-c(RGDfC) **22** and **23** display very modest inhibitory activities (IC_{50} >250 µM, entries 5 and 6). These findings are in line with the binding properties of *O*-glyco"RGD" previously synthesized in our group.

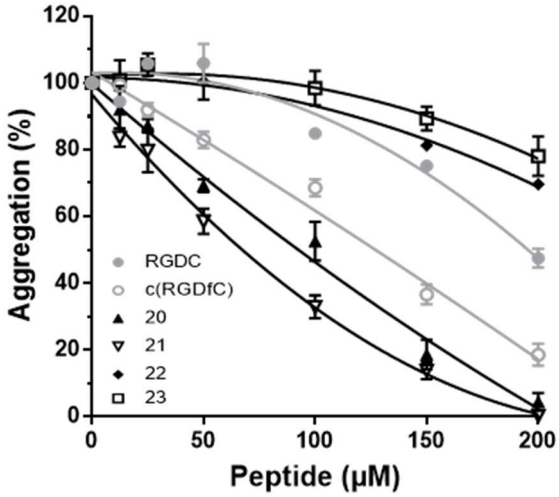

Fig 2. Effect of *C*-glyco"RGD" **20**-**23** and reference peptides on human platelet aggregation in response to ADP. The results are the means ± SEM of 4 to 5 independent experiments with PRP from different donors.

The activity of the *C*-glyco"RGD" against $\alpha_v\beta_3$ integrins was also evaluated in a cell adhesion assay. The inhibition of the $\alpha_v\beta_3$ integrin-dependent adhesion of VSMCs to plates pre-coated with vitronectin was tested. Linear *C*-glyco-RGDC **20**-**21** and RGDC showed poor vitronectin displacement (Fig 3a). As shown in table 1, these compounds displayed the lowest inhibitory activities (IC_{50} >2000 µM, entries 1, 3 and 4). The cyclic derivatives *C*-glyco-c(RGDfC) **22**-**23** and c(RGDfC) prominently reduced adhesion in a dose-dependent manner (Fig 3b). These cyclic compounds were the most potent inhibitors and displayed similar IC_{50} values in the low micromolar range (2.8 to 9.3 µM, entries 2, 5 and 6).

Table 1
Inhibition of ADP-induced platelet aggregation and VSMC adhesion to vitronectin

Entry	Peptide	IC_{50} (µM)	
		Platelet aggregation	VSMC adhesion
1	RGDC **16**	223 ± 11	> 2000
2	*c*(RGDfC) **17**	139 ± 6	2.8 ± 0.7
3	**20**	100 ± 5	> 2000
4	**21**	65 ± 7	> 2000
5	**22**	> 250	4.4 ± 0.6
6	**23**	> 250	9.3 ± 0.6

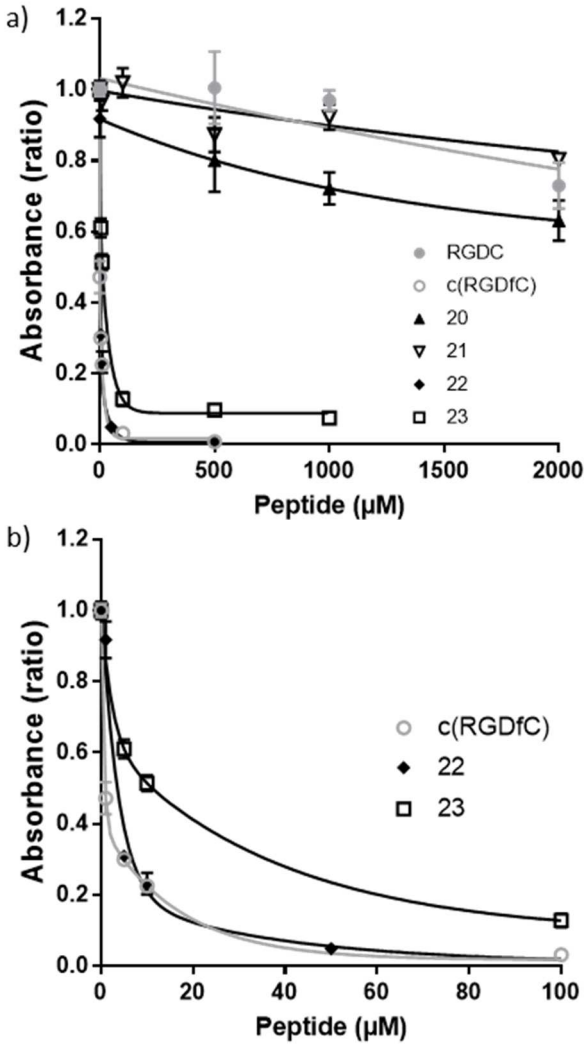

Fig 3. a) Effect of *C*-glyco"RGD" **20**-**23** and reference peptides on human VSMC adhesion to immobilized vitronectin. The results are the means ± SEM of 4 to 5 independent experiments. b) Zoom for 0-100 µM peptide concentration.

The *in vitro* stability of *C*-glyco"RGD" was determined using a routine protocol notably used in molecular imaging.[27] The stability of these conjugates was determined in human serum *in vitro* at 37°C by HPLC monitoring. HPLC analysis of acetonitrile serum extracts at different incubation time points during the incubation period of 120 minutes demonstrating the in vitro stability of those tools built with a stable *C*-glycoside.

2.3. Molecular-dynamics simulations.

We built molecular models of a linear and a cyclic *C*-glyco"RGD", using compounds **20** and **22** respectively. The initial 3D structures were first built using the Molefacture plugin of VMD[59] and subsequently solvated in a bath of explicit water. To rationalize the biological profile of *C*-glyco-c(RGDfC) **22** toward $\alpha_v\beta_3$, a molecular assay of the integrin in complex with the cyclic c(RGDfC) was further built. We started from the crystal structure of the extracellular segment of integrin $\alpha_v\beta_3$ in complex with cyclic peptide c(RGDfV) (PDB:1L5G).[60] For the protein, missing residues were not incorporated, similarly to the work of Xiong et al.[61] Two molecular assays were constructed using either the crystal RGD peptide or the cyclic *C*-glyco-c(RGDfC) **22**. The complex involving the latter ligand was generated by aligning its c(RGDfC)

moiety onto the RGD structure of the peptide in the crystal. Finally, a solution of 150 mM NaCl was added to simulation boxes (Fig 4).

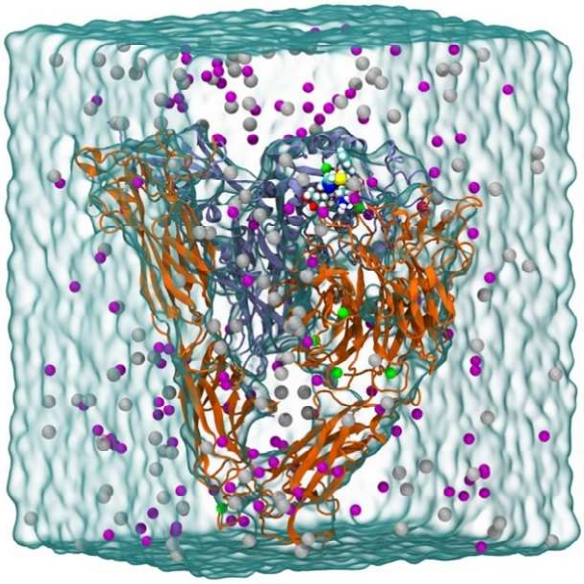

Fig 4. Initial simulation box for the cyclic *C*-glyco"RGD" **22** in complex with the extracellular segment of integrin $\alpha_v\beta_3$ (PDB:1L5G). Chlorine, sodium and magnesium ions are depicted by violet, grey and green van der Waals spheres respectively. Water molecules are represented by the cyan molecular surface. Orange and ice blue cartoons stand for the integrin propeller and βA domains respectively. The RGD ligand is represented by van der Waals sphere colored by atom name (oxygen: red, hydrogen: white, sulfur: yellow, nitrogen: blue and carbon: cyan)

The conformational dynamics of the linear and the cyclic *C*-glyco"RGD" **20** and **22** differs markedly in solution. The cycle formed by the c(RGDfC) backbone is essentially rigid along the MD trajectory while the spacer arm carrying the carbohydrate group remains predominantly in an extended conformation, preventing intramolecular interactions. Consequently, the glyco moiety moves in a well-defined volume opposite to the RGD sequence and extending from the arginine to the phenylalanine side chains (Fig 5). At variance, the linear *C*-glyco-RGDC appears more flexible navigating between various conformations mainly characterized by the formation of intramolecular interactions. The most frequent conformation observed during the simulation involves an electrostatic interaction between the arginine side chain and the terminal carboxylate of the cysteine residue, resulting in a cyclic-like arrangement of the RGD sequence. The space-volume being accessed by the carbohydrate group is larger than in the case of the cyclic ligand (Fig 5), suggesting a higher plasticity.

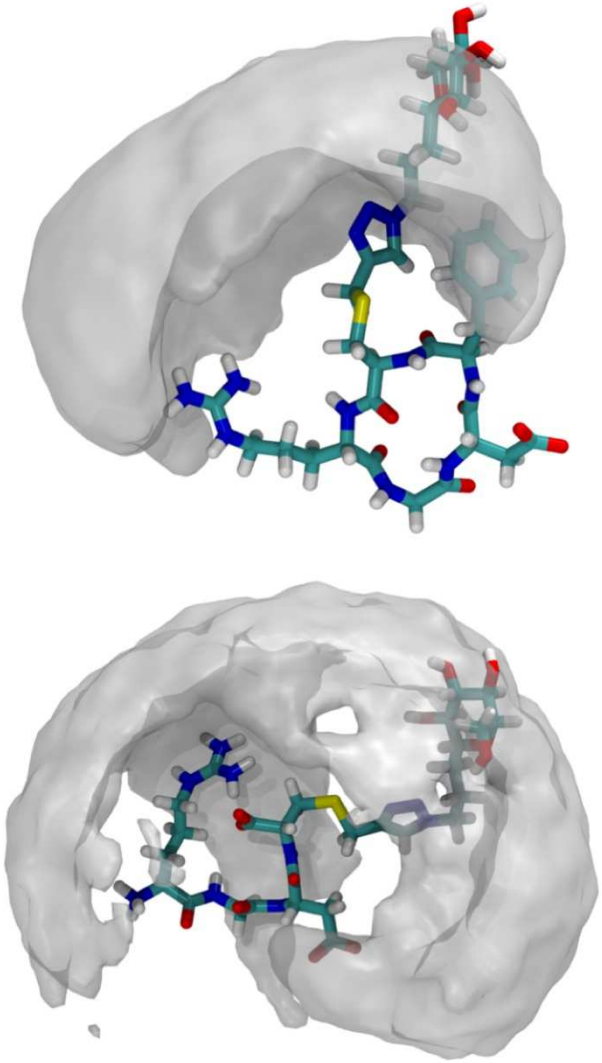

Fig 5. Representative snapshots of (top) cyclic *C*-glyco-c(RGDfC) **22** and (bottom) linear *C*-glyco-RGDC **20** extracted from the 500 ns-long molecular-dynamics simulations of the free ligands in water. The RGD ligand is represented by licorices colored by atom name. Semi-transparent white surface represents an isosurface of the mass-weighted atomic density of the carbohydrate moiety computed over the MD trajectory with the VolMap plugin of VMD.

Binding of compound **22** (IC_{50} = 4.4 μM) and reference c(RGDfC) **17** (IC_{50} = 2.8 μM) to the extracellular domain of $\alpha_v\beta_3$ integrin was investigated using MD simulations (Fig 6). The RGD/integrin interface observed all along the 500 ns-long trajectories remains essentially the same for both peptides. More specifically, the aspartic acid of the ligand interacts tightly with a magnesium ion, the latter being strongly associated to S121, S123 and E220. It further forms a hydrogen bond with the backbone of Y122. The arginine is forming a robust salt-bridge with D218 irrespective of the interacting compound. The in-silico experiments further highlighted that the glyco-moiety of compound **22** interacts transiently with the βA domain of the integrin, most often with charged residues K125 and D126.

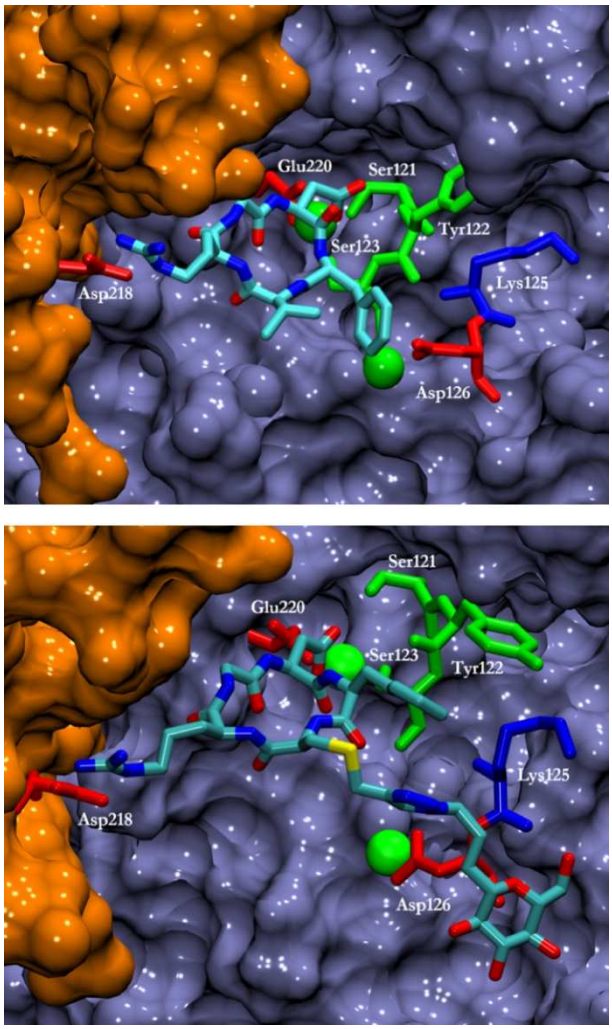

Fig 6. Representative snapshots of the binding interface of $\alpha_v\beta_3$ integrin and (top) cyclic c(RGDfC) and (bottom) cyclic *C*-glyco-c(RGDfC) **22** extracted from the 500 ns-long molecular-dynamics simulations. Integrin propeller and βA domains are depicted by orange and ice blue surfaces respectively. Magnesium ions are represented by green van der Waals spheres. Integrin amino acids interacting with the peptide are colored by residue type (polar: green, acidic: red and basic: blue). The RGD ligand is represented by licorices colored by atom name (hydrogens are omitted for clarity).

3. Discussion

The development of high affinity and selective ligands toward integrins for in vivo applications like molecular imaging remains a daunting challenge. RGD binding regions are very similar in most integrins, it is thus not easy to design ligands exhibiting simultaneously high selectivity and high affinity for distinct subtypes. Nevertheless, this is an essential requirement for the use of bioactive molecules in molecular imaging.[16,58] Of equal importance is bioavailability, especially in the context of PET imaging relying on radioisotopes of short half-life. In this contribution, we have designed original linear and cyclic *C*-glyco"RGD" tools which possess a carbohydrate moiety bearing a fluorine atom, making them suitable for future applications in PET imaging. The radiosynthesis of these conjugates was performed to produce four [^{18}F]fluoro-C-glyco"RGD" ready to be investigated in PET imaging. The introduction of a three-carbon triazolyl linker provides a rather high flexibility to the synthetized ligands. Molecular simulations revealed that, in solution, the carbohydrate group explores an ensemble of conformations irrespective of the topology (cyclic or linear) of the RGD peptides, however subtle differences in the flexibility of the linear and cyclic conjugates may be highlighted. Such a conformational dynamic is anticipated to modulate their level of affinity and selectivity towards $\alpha_{IIb}\beta_3$ and $\alpha_v\beta_3$ integrins. Of particular importance, the introduction of a C-C bond to link the *C*-glycoside prosthetic group increases significantly the resistance to proteolytic degradation compared to *O*-glycoside derivatives that were developed previously.[19,34] The stability of the latter compounds was shown to be limited to one hour *in vitro*, a time range suboptimal for PET imaging. At variance, *C*-glycoside derivatives remain stable for two hours in human serum, making them perfect candidates towards *in vivo* imaging application.

Testing the efficacy of integrin ligands in the cellular context is a difficult endeavor. There is no consensual protocol to measure unambiguously the binding affinity of RGD-ligands towards integrins, making the comparison of the ensemble of published data hazardous.[16] In an effort to reconcile the various binding studies, Kessler et al. have evaluated systematically the affinity of a wide range of ligands towards integrins using a unique solid phase binding assay.[16] Here, the biological effect on $\alpha_{IIb}\beta_3$ and $\alpha_v\beta_3$ integrins were examined using functional tests. While the binding affinity of RGD peptide derivatives can be accurately measured using a solid phase binding assay, their ability to modulate biological functions has to be also assessed to evaluate their relevance as diagnostic tools. Previous studies with integrin antagonists and knockout mice have clearly demonstrated that $\alpha_{IIb}\beta_3$, the most abundant integrin expressed on platelets and whose expression is restricted to cells of the megakaryocyte lineage, is a crucial adhesive receptor for platelet aggregation.[62] A key feature of vascular cells is their adhesive status which is determined by a repertoire of adhesion receptors. In the vascular wall the αv subunit pairs with β_1, β_3, β_5, β_6 and β_8 that play different roles in attachment and migration, but the αv subunit only pairs with the β_3 subunit on the surface of VSMCs[63] and only $\alpha_v\beta_3$ interacts with all major matrix ligands.[64] The first identified function of $\alpha_v\beta_3$ was its capacity to mediate attachment of cells including VSMCs to vitronectin. Therefore, inhibition of platelet aggregation and inhibition of VSMC adhesion to vitronectin are highly relevant assays to identify RGD derivatives that can be further used as functional probes.

The addition of a *C*-glycoside moiety on either a linear or a cyclic RGD scaffolds affects their binding to $\alpha_{IIb}\beta_3$ and $\alpha_v\beta_3$ integrins in a different manner. While cyclic ligands **22** and **23**, demonstrate promising affinity for $\alpha_v\beta_3$, it was not the case towards $\alpha_{IIb}\beta_3$, in sharp contrast with the affinity reported for standard cyclic-RDGs.[16] Interestingly enough, linear conjugates **20** and **21** displayed only weak affinity to $\alpha_v\beta_3$, following the trend observed for non-functionalized linear RGDs, but their inhibitory affinities toward $\alpha_{IIb}\beta_3$ is highly enhanced by the addition of a carbohydrate group and the chemical linker. The peculiar biological profile of *C*-glyco"RGD" can be rationalized by analyzing their structural dynamics and the topology of the binding pockets of $\alpha_v\beta_3$ and $\alpha_{IIb}\beta_3$. For the latter integrin the binding site appears more ensconced compare to that of $\alpha_v\beta_3$, as revealed by of X-Ray crystallography (PDB:1LG5 and PDB:3ZE2) (see Figure S20 for a side-by-side comparison of the two binding sites). Molecular-dynamics simulation clearly shows that the linear peptide is much more flexible than its cyclic homolog, allowing to adapt to the somewhat buried cavity of $\alpha_{IIb}\beta_3$, whereas the more rigid cyclic compound is anticipated to be sterically hindered preventing its binding to this integrin. However, the relative rigidity of the cyclic *C*-glyco-c(RGDfC) does not impair its recognition by the flatter binding site of $\alpha_v\beta_3$. Molecular-dynamics simulation performed on the most potent compound **22** show that the RGD/integrin interface remains essentially the same for **22** and native c(RGDfC) **17**. The in-silico experiments further highlight that the glyco-moiety

of compound **22** interacts transiently with the βA domain of the integrin, most often with charged residues K125 and D126, rationalizing possibly the higher affinity of the conjugated compared to its native analog.

4. Conclusion

Four new 6-fluoro-*C*-glyco"RGD" tools aimed at targeting integrins for molecular imaging purposes have been synthesized and radiosynthesized by conjugating RGD peptide derivatives with 6-fluorosugars via a triazolyl moiety. The design of all the derivatives has exploited the robustness and hydrophilicity of *C*-glycosides to enhance their possible efficiency, while a three-carbon flexible spacer was selected in order to minimize the steric hindrance. Remarkably, distinct affinity profiles towards $\alpha_{IIb}\beta_3$ and $\alpha_v\beta_3$ integrins can be achieved by modulating the RGD conjugates topology. Indeed, the linear *C*-glyco-RGDC **20** and **21** showed a notable effect for $\alpha_{IIb}\beta_3$ while cyclic *C*-glyco-c(RGDfC) **22** and **23** preferentially bind to $\alpha_v\beta_3$ with an IC_{50} of 4.4 and 9.3 µM respectively. Important effects on cell adhesions have been highlighted. Molecular modeling and simulation rationalized the distinct biological properties of *C*-glyco"RGD" and in particular the preference of cyclic *C*-glyco-c(RGDfC) **22** in the targeting $\alpha_v\beta_3$ integrin due to a combined effect of the ligand flexibility and of the integrin binding pocket hindrance. The achievement of this distinct affinity profile is clearly of crucial results that will show all its importance for *in vivo* applications. Our results allow us to propose the use of the linear [^{18}F]F-*C*-glyco-RGDC **[^{18}F]20** and **[^{18}F]21** for thrombosis imaging, while the cyclic [^{18}F]F-*C*-glyco-c(RGDfC) **[^{18}F]22** and **[^{18}F]23** could be promising tools for cancer diagnosis.

5. Experimental section

5.1. Materials and methods

Solvents and liquid reagents were purified and dried according to recommended procedures. Thin layer chromatography (TLC) analyses were performed using standard procedures on Kieselgel 60F254 plates (Merck, Kenilworth, NJ, USA). Compounds were visualized using UV light (254 nm) and a methanolic solution of sulfuric acid and charred. Column chromatography was performed on silica gel SI 60 (63–200 µm) (Merck). Purification of glyco-conjugates was achieved by gel filtration on LH20 using water or water/methanol mixture as eluent. Melting points were determined with a Tottoli apparatus and are uncorrected. FTIR spectra were recorded on a Shimadzu IRAffinity-1, ATR PIKE Technologies model GladiAT (cm-1). Optical rotations were measured on an Anton-Paar MCP 300 polarimeter. Analytical High performance liquid chromatography (HPLC) analyses were run on a Waters system (2695eb pump, auto sampler injector, 2998 PDA detector, 2424 ELSD detector, and NaI detector from Berthold [Bad Wildbad, Germany]) controlled by the Empower Software (Orlando, FL, USA). Analyses were performed on a Vydac 218TP C18 (5 µm, 250 × 4.6 mm) from Grace or Alltima C8 (5 µm, 150 × 4.6 mm) from Grace with ACN/H2O/TFA mixture (proportions given in brackets) at 1 mL/min. Integrated HPLC system on AllInOne synthesizer was equipped with a radioactivity detector, Smartline UV detector 200 (Knauer, Berlin, Germany) at 254 nm and a HPLC pump P4.1.5 (Knauer, Berlin, Germany). Semi-preparative HPLC were performed on an Alltima C8 endcapped (5µm, 150×10 mm) from Grace (HPLC n°1) and on a Vydac 218TP C18 (5 µm, 250x10mm) from Grace (HPLC n°2) with ACN/H_2O or ACN/H_2O/TFA mixture (proportions given in brackets) at 4.5 or 3 mL/min respectively. 1H, 13C, and 19F NMR spectra were recorded on a Bruker spectrometer DPX250 (250 MHz, 62.9 MHz and 235 MHz, respectively) or Avance III 400 (400 MHz and 100.6 MHz, respectively). For complete assignment of 1H and 13C signals, two-dimensional 1H, 1H COSY and 1H, 13C correlation spectra were recorded. Chemical shifts (δ) are given in parts per million relative to the solvent residual peak. For clarity, atom numbering starts from the end of the anomeric arm rather than resulting from the IUPAC naming of compounds (cf fig S1). The following abbreviations are used for multiplicity of NMR signals: s = singlet, d = doublet, t = triplet, q = quadruplet, m = multiplet, b = broad signal and app = apparent multiplicity. The given J values refer to apparent multiplicities and do not represent the true coupling constants. Mass and high resolution mass spectrometry spectra were recorded on a Bruker microTOFQ apparatus. No-carrier-added fluoride-18 was produced via the ^{18}O (p,n)^{18}F nuclear reaction on a PET Trace cyclotron (GE). The bombardment was performed at 10 µA during 5 minutes to provide about 5 GBq of fluoride-18 delivered as a solution in ^{18}O-enriched water (1.6 mL). Radiosynthesis was carried out on an AIO module from Trasis®.

5.2. Experimental procedure and physico-chemical characterization

Compounds **2**, **3**[47] **4**, **6**[55] and **18**, **19**[19] were prepared according to previously described methods.

Complete experimental details and physico-chemical characterization of new compounds, biological assays and molecular-dynamics simulation protocols are described in the supporting information part.

5.2.1. General method for the synthesis of fluoro-C-glyco"RGD"

To a solution of S-propargyl derivative **18** and **19** (0.02 mmol) and azido derivatives **14** or **15** (0.02 mmol) diluted in water (0.4mL), was added at room temperature sodium ascorbate (0.004 mmol) in water (0.4 mL) and a solution of $Cu(OAc)_2$ (0.002 mmol) in water (0.045 mL). The solution turned immediately pale green. The reaction was stopped when the intense blue color reappeared (2h of stirring). Chelex® resin (150 mg) was then added to the blue solution and the suspension was stirred until the solution turned colorless. The resin was filtered off and the resulting solution was freeze-dried. Purification was achieved on Sephadex LH20 resin. Elution with water provided pure fluoro *C*-glycopeptides **20**, **21**, **22** or **23**. For c(RGDfC) **19**, 0.005 mmol of peptide was introduced, proportion of other reactive was respected.

*5.2.2. L-Cysteine,L-arginylglycyl-L-α-aspartyl-S-[[1-[1-(4,8-anhydro-5-fluoro-5,1,2,3-trideoxy-D-glycero-D-gulo-nonitol)]-1H-1,2,3-triazol-4-yl]methyl] (**20**)*

Yield 74%. White foam. $[\alpha]_D$: + 4.9 (*c* 0.05; H_2O). ^{1}H NMR (400 MHz, D_2O): δ 1.40-1.50 (m, 1H, H3a), 1.70-1.88 (m, 3H, H2a and CH_2), 1.96-2.22 (m, 4H, H2b, H3b and CH_2), 2.60-2.75 (m, 1H, ½CH_2), 2.77-3.06 (m, 3H, ½CH_2 and CH_2), 3.15-3.35 (m, 4H, H4, H5 and CH_2), 3.44-3.57 (m, 3H, H6, H7 and H8), 3.83-4.20 (m, 4H, 2 CH_2), 4.39 (bs, 1H, CH), 4.45-4.70 (m, 5H, H1, H9 and 2 CH), 8.06 (bs, 1H, $H_{triazole}$). ^{13}C NMR (100.6 MHz, D_2O): δ 23.4 (CH_2), 25.4 (C2 and CH_2), 27.7 (C3), 28.0 (CH_2), 33.3 (CH_2), 40.4 (2 CH_2), 42.5 (CH_2), 50.3 (C1), 51.6 (CH), 52.8 (CH), 54.3 (CH), 68.6 (d, $J_{C,F}$ = 7.0 Hz, C7), 73.3 (C5), 77.2 (C6), 78.0 (d, $J_{C,F}$ = 17.0 Hz, C8), 78.9 (C4), 82.3 (d, $J_{C,F}$ = 168.0 Hz, C9), 125.2 ($CH_{triazole}$), 140.8 ($C_{triazole}$), 156.8 (C=N), 170.1 (C=O), 170.7 (2

C=O), 172.4 (C=O), 176.2 (C=O). ^{19}F NMR (235 MHz, D_2O): δ - 234.8. HRMS (ESI, $C_{26}H_{43}FN_{10}O_{11}SH$: $[M + H]^+$) calcd 737.3052, found 737.3005. HPLC purity: 97.5%.

*5.2.3. L-Cysteine,L-arginylglycyl-L-α-aspartyl-S-[[1-[9-(2,6-anhydro-1-fluoro-1,7,8,9-trideoxy-D-glycero-L-gulo-nonitol)]-1H-1,2,3-triazol-4-yl]methyl] (**21**)*

Yield 71%. White foam. $[\alpha]_D$: -7.6 (*c* 0.07; H_2O). ^{1}H NMR (400 MHz, D_2O): δ 1.53-1.74 (m, 4H, H3a, H2a and CH_2), 1.77-1.88 (m, 2H, CH_2), 1.88-1.98 (m, 1H, H2b), 2.00-2.14 (m, 1H, H3b), 2.62 (dd, 1H, *J* = 16.0 Hz, *J* = 8.5 Hz, ½CH_2), 2.73 (dd, 1H, *J* = 16.0 Hz, *J* = 4.5 Hz, ½CH_2), 2.86 (dd, 1H, *J* = 14.0 Hz, *J* = 7.0 Hz, ½CH_2), 2.97 (dd, 1H, *J* = 14.0 Hz, *J* = 4.5 Hz, ½CH_2), 3.12-3.30 (m, 3H, H5 and CH_2), 3.34-3.47 (m, 1H, H8), 3.43 (app t, 1H, $J_{7,6}$ = $J_{7,8}$ = 9.5 Hz, H7), 3.59 (app t, 1H, $J_{6,5}$ = $J_{6,7}$ = 9.5 Hz, H6), 3.71 (dd, 1H, *J* = 9.5 Hz, *J* = 6.0 Hz, H4), 3.87 (s, 2H, CH_2), 3.96 (d, 1H, *J* = 16.5 Hz, ½CH_2), 3.99-4.06 (m, 1H, CH), 4.12 (d, 1H, *J* = 16.5 Hz, ½CH_2), 4.35 (dd, 1H, *J* = 7.0 Hz, *J* = 4.5 Hz, CH), 4.49 (t, 2H, $J_{1,2}$ = 7.0 Hz, H1), 4.65 (bd, 2H, $J_{H9,F}$ = 47.0 Hz, H9), 4.67 (dd, 1H, *J* = 8.5 Hz, *J* = 5.0 Hz, CH), 7.98 (bs, 1H, $H_{triazole}$). ^{13}C NMR (100.6 MHz, D_2O): δ 20.3 (CH_2), 23.7 (CH_2), 25.2 (C2), 25.5 (C3), 29.8 (CH_2), 33.2 (CH_2), 38.3 (CH_2), 40.6 (CH_2), 42.4 (CH_2), 49.9 (C1), 51.5 (CH), 52.8 (CH), 54.2 (CH), 68.9 (d, $J_{C,F}$ = 7.0 Hz, C7), 70.9 (C5), 71.1 (d, $J_{C,F}$ = 17.0 Hz, C8), 72.3 (C6), 75.6 (C4), 82.4 (d, $J_{C,F}$ = 168.0 Hz, C9), 124.2 ($CH_{triazole}$), 138.4 ($C_{triazole}$), 156.7 (C=N), 170.9 (C=O), 172.5 (2C=O), 174.6 (C=O), 176.3 (C=O). ^{19}F NMR (235 MHz, D_2O): δ - 234.7. HRMS (ESI, $C_{26}H_{43}FN_{10}O_{11}SH$: $[M + H]^+$) calcd 737.3052, found 737.3055. HPLC purity: 99.0%.

*5.2.4. Cyclo[L-arginylglycyl-L-α-aspartyl-D-phenylalanyl-S-[[1-[1-(4,8-anhydro-5-fluoro-5,1,2,3-trideoxy-D-glycero-D-gulo-nonitol)]-1H-1,2,3-triazol-4-yl]methyl]-L-cysteinyl] (**22**)*

Yield 69%. White foam. $[\alpha]_D$: +6.3 (c 0.05; H_2O). ^{1}H NMR (400 MHz, D_2O): δ 1.42-1.64 (m, 3H, H3a, H2a and ½CH2), 1.65-1.77 (m, 1H, H2b), 1.81-1.93 (m, 2H, H3b, ½CH2), 2.00-2.23 (m, 2H, CH_2), 2.55 (dd, 1H, *J* = 16.0 Hz, *J* = 7.0 Hz, ½CH_2), 2.68 (dd, 1H, *J* = 16.0 Hz, *J* = 7.0 Hz, ½CH_2), 2.75 (bd, 1H, *J* = 7.0 Hz, ½CH_2), 3.00-3.13 (m, 1H, ½CH_2), 3.16-3.26 (m, 3H, H5 and CH_2), 3.33 (app td, 1H, $J_{4,5}$ = 9.5 Hz, $J_{4,3}$ = 3.0 Hz, H4), 3.45-3.56 (m, 4H, H6, H7, H8 and CH), 3.71 (s, 2H, CH_2), 4.19-4.27 (m, 2H, CH_2), 4.41 (dd, 1H, *J* = 9.0 Hz, *J* = 6.0 Hz, CH), 4.48-4.52 (m, 2H, H1), 4.61-4.77 (m, 6H, CH_{2benz}, H9 and 2CH), 7.26-7.39 (m, 5H, H_{Ar}), 7.91 (s, 1H, H-triazole). ^{13}C NMR (100.6 MHz, D_2O): δ 24.5 (C2), 25.2 (CH_2), 25.5 (CH_2), 27.1(CH_2), 27.7 (C3), 36.4 ($2CH_2$), 40.5 ($2CH_2$), 43.7 (CH_2), 50.2 (C1), 50.8 (CH), 52.7 (CH), 54.3 (CH), 55.2 (CH), 68.6 (d, $J_{C,F}$ = 7.0 Hz, C7), 73.3 (C5), 77.2 (C6), 78.1 (d, $J_{C,F}$ = 17.0 Hz, C8), 78.9 (C4), 82.4 (d, $J_{C,F}$ = 168.0 Hz, C9), 124.0 ($CH_{triazole}$), 127.1(C_{Ar}), 128.8 ($2C_{Ar}$), 129.2 ($2C_{Ar}$), 136.1(C_{qAr}), 144.6 ($C_{triazole}$), 156.8 (C=N), 171.2 (2C=O), 172.3 (C=O), 172.6 (C=O),173.3 (C=O), 177.9 (C=O). ^{19}F NMR (235 MHz, D_2O): δ - 234.6. HRMS (ESI, $C_{36}H_{53}FN_{11}O_{11}SH$: $[M + H]^+$) calcd 866.3631, found 866.3680. HPLC purity: 99.2% (305 nm).

*5.2.5. Cyclo[L-arginylglycyl-L-α-aspartyl-D-phenylalanyl-S-[[1-[9-(2,6-anhydro-1-fluoro-1,7,8,9-trideoxy-D-glycero-L-gulo-nonitol)]-1H-1,2,3-triazol-4-yl]methyl]-L-cysteinyl] (**23**)*

Yield 65%. White foam. $[\alpha]_D$: -9.7 (c 0.1; H_2O). ^{1}H NMR (400 MHz, CD_3OD): δ 1.56-1.86 (m, 6H, H3a, H2a and $2CH_2$), 1.92-2.06 (m, 1H, H2b), 2.10-2.19 (m, 1H, H3b), 2.62 (dd, 1H, *J* = 16.0 Hz, *J* = 7.5 Hz, ½CH_2), 2.74 (dd, 1H, *J* = 16.0 Hz, *J* = 7.0 Hz, ½CH_2), 2.81 (d, 1H, *J* = 7.0 Hz, ½CH_2), 3.08-3.20 (m, 2H, CH_2), 3.23-3.33 (m, 2H, H5 and ½CH_2), 3.50-3.61 (m, 3H, H4, H6 and H7), 3.67-3.83 (m, 4H, H8, CH and CH_2), 4.04-4.15 (m, 2H, 2CH), 4.25-4.33 (m, 2H, CH_2), 4.47 (dd, 1H, *J* = 9.0 Hz, *J* = 5.5 Hz, CH), 4.58 (t, 2H, *J* = 7.0 Hz, H1), 4.66-4.87 (m, 4H, CH_{2benz} and H9), 7.32-7.36 (m, 3H, H_{Ar}), 7.41-7.45 (m, 3H, H_{Ar}), 7.99 (s, 1H, $H_{triazole}$). ^{13}C NMR (100.6 MHz, CD_3OD): δ 21.7 (CH_2), 24.4 (CH_2), 25.6 (C2), 26.3 (C3), 26.8 (CH_2), 37.6 (CH_2), 39.0 (CH_2), 41.7 ($2CH_2$), 44.8 (CH_2), 51.2 (C1), 52.0 (CH), 53.9 (CH), 55.5 (CH), 56.3 (CH), 64.1 (C5), 70.1 (d, $J_{C,F}$ = 8.0 Hz, C7), 72.1 (d, $J_{C,F}$ = 17.0 Hz, C8), 73.5 (C6), 74.0 (C4), 82.5 (d, $J_{C,F}$ = 168.0 Hz, C9), 125.1 (CHtriazole), 128.3 (CAr), 129.9 (2CAr), 130.3 (2CAr), 137.3 (CqAr), 143.7 (Ctriazole), 162.0 (C=N), 172.2 (2C=O), 172.4 (C=O), 173.7 (C=O), 173.7 (C=O), 179.0 (C=O). ^{19}F NMR (235 MHz, D2O): δ - 234.6. HRMS (ESI, $C_{36}H_{53}FN_{11}O_{11}SNa$: $[M + Na]^+$) calcd 888.3450, found 888.3277. HPLC purity: 99.7% (209 nm).

Acknowledgment

This work was supported by Institut Jean Barriol and the Investments for the Future program under grant agreement No ANR-15-RHU-0004. We acknowledge The Ministère de l'Enseignement Supérieur et de la Recherche for PhD funding to T. Vucko. We acknowledge the State-Region Plan "Technological Innovations, Modeling and Personalized Medical Support" (IT2MP) and the European Regional Development Funds (ERDF) for generous support. We thank S. Adach, F. Lachaud and P. Ponce for technical assistance.

References

1. Carmeliet, P. Angiogenesis in life, disease and medicine. *Nature* **2005**, *438*, 932-936.
2. Ribatti, D. History of research on angiogenesis. *Chem Immunol Allergy*. **2014**, *99*, 1-14.
3. Folkman, J. Role of angiogenesis in tumor growth and metastasis. *Semin. Oncol*. **2002**, *29*, 15–18.
4. Barczyk, M., Carracedo, S., and Gullberg, D. Integrins. *Cell Tissue Res*. **2010**, *339*, 269-280.
5. Luo, B.-H., Carmen, C., and Springer, T. Structural basis of integrin regulation and signalling. *Annu. Rev. Immunol*. **2007**, *25*, 619-647.
6. For a review see: Durrant, T. N., van den Bosch, M. T., and I. Hers. Integrin αIIbβ3 outside-in signaling. *Blood* **2017,** *130*, 1607–1619.
7. Miller, L. M., Pritchard, J. M., Macdonald, S. J. F., Jamieson, C., and Watson, A. J. B. Structure-activity relationships of small molecule autotaxin inhibitors with a discrete binding mode. *J. Med. Chem.* **2017**, *60*, 3241–3251
8. Raab-Westph, S., Marshall, J. F., and Goodman, S. L. Integrins as Therapeutic Targets: Successes and Cancers. *Cancers* **2017**, *9*, 110-138.
9. Demircioglu, F., and Hodivala-Dilke, K. αvβ3 Integrin and tumour blood vessels-learning from the past to shape the future. *Curr. Opin. Cell Biol*. **2016**, *42*, 121-127
10. Nieberler, M., Reuning, U., Reichart, F., Notni, J., Wester, H.-J., Schwaiger, M., Weinmüller, M., Räder, A., Steiger, K., and Kessler, H. Exploring the Role of RGD-Recognizing Integrins in Cancer. *Cancers* **2017**, *9*, 116-149.
11. Fong, K. P., Zhu, H., Span, L. M., Moore, D. T., Yoon, K, Tamura, R, Yin, H., DeGrado, W. F., and Bennett, J. Directly

Activating the Integrin αIIbβ3 Initiates Outside-In Signaling by Causing αIIbβ3 Clustering. *J. Biol. Chem*. **2016**, *291*, 11706-11716.
12. Deckmyn, H., De Meyer, S. F., Broos, K., and Vanhoorelbeke, K. Inhibitors of the Interactions Between Collagen and Its Receptors on Platelets, Gresele, P., Born, G. V. R., Patrono, C., Page, C. P. Eds., Handbook of Experimental Pharmacology: Antiplatelets Agents, Springer, **2012**, 311-337.
13. Pierschbacher, M.D., and Ruoslahti, E. Cell attachment activity of fibronectin can be duplicated by small synthetic fragments of the molecule, *Nature* **1984**, *309*, 30–33.
14. Hatley, R. J. D, Macdonald, S. J. F., Slack, R. J., Le, J., Ludbrook, S. B., and Lukey P. T. An αv-RGD Integrin Inhibitor Toolbox: Drug Discovery Insight, Challenges and Opportunities. *Angew. Chem. Int. Ed*. **2018**, *57*, 2–26.
15. Duro-Castano, A., Gallon, E., Decker, C., and Vicent, M. J. Modulating angiogenesis with integrin-targeted nanomedicines. *Adv. Drug. Deliv. Rev*. **2017**, *119*, 101-119.
16. Kapp, T. G., Rechenmacher, F., Neubauer, S., Maltsev, O. V., Cavalcanti-Adam, E. A., Zarka, R., reuning, U., Notni, J., Wester, H. J., Mas-Moruno, C., Spatz, J., Geiger, B., and Kessler, H. A Comprehensive Evaluation of the Activity and Selectivity Profile of Ligands for RGD-binding Integrins. *Sci. Rep.* **2017***, 7*, 39805-39821.
17. Gaertner, F. C., Kessler, H., Wester, H. J., Schwaiger, M., and Beer, A. J. Radiolabelled RGD peptides for imaging and therapy. *Eur. J. Nucl. Med. Mol. Imaging* **2012**, *39*, 126–138.
18. For a review see: Chen, H., Niu, G., Wu, H., Chen, X. Clinical Application of Radiolabeled RGD Peptides for PET Imaging of Integrin αvβ3. *Theranostics* **2016**, *6*, 78–92.
19. Lamandé-Langle, S., Collet, C., Hensienne, R., Vala, C., Chrétien, F., Chapleur, Y., Mohamadi, A., Lacolley, P., and Regnault, V. "Click" glycosylation of peptides through cysteine propargylation and CuAAC. *Bioorg. Med. Chem*. **2014,** *22,* 6672-6683.
20. Zhou, Y., Chakrabortv, S., and Liu, S. Radiolabeled cyclic RGD peptides as radiotracers for imaging tumors and thrombosis by SPECT. *Theranostics* **2011**, *1*, 58–82.
21. for a review see: Nguyen, J.-T., and Kiso, Y. Delivery of peptide drugs, Dunn, B. M. Eds. Peptide Chemistry and Drug De-sign, Wiley, **2015**, 271-310.
22. Moradi, S. V., Hussein, W. M., Varamini, P., Simerskaa, P., and Toth, I. Glycosylation, an effective synthetic strategy to improve the bioavailability of therapeutic peptides. *Chem. Sci*. **2016**, *7*, 2492-2500.
23. Haubner, R., Kuhnast, B., Mang, C., Weber, W. A., Kessler, H., Wester, H. J., and Schwaiger, M. [18F]Galacto-RGD: synthesis, radiolabeling, metabolic stability, and radiation dose estimates. *Bioconjugate Chem.* **2004**, *15*, 61–69.
24. Pratta, M. R., and Bertozzi, C. R. Synthetic glycopeptides and glycoproteins as tools for biology. *Chem. Soc. Rev*. **2005**, *34*, 58–68.
25. Grogan, M. J., Pratt, M. R., Marcaurelle, L. A., and Bertozzi, C. R. Homogeneous Glycopeptides and Glycoproteins for Biological Investigation. Annu. Rev. Biochem. 71, 593–634.
26. Chapleur, Y., Vala, C., Chrétien, F., and Lamandé-Langle, S. (2013) Toward imaging glycotools by click coupling in Click Chem-istry in Glycoscience: New Developments and strategies, Witczak, Z. J., Bielski, R., Eds, Wiley, **2002**, pp 183-210.
27. Maschauer, S., Haubner, R., Kuwert, T., and Prante, O. (18)F-glyco-RGD peptides for PET imaging of integrin expression: efficient radiosynthesis by click chemistry and modulation of biodistribution by glycosylation. *Mol. Pharm.* **2014**, *11*, 505–515.
28. Gaertner, F. C., Kessler, H., Wester, H. J., Schwaiger, M., and Beer, A. J. Radiolabelled RGD peptides for imaging and therapy. *Eur. J. Nucl. Med. Mol. Imaging* **2012,** *39*, 126-38.
29. Haubner, R., Wester, H.-J., Weber, W. A., Mang, C., Ziegler, S. I., Goodman, S. L., Senekowitsch-Schmidtke, R., Kessler, H., and Schwaiger M. Noninvasive Imaging of avb3 Integrin Expression Using 18F-labeled RGD-containing Glycopeptide and Positron Emission Tomography. *Cancer Res*. **2001**, *61*, 1781–1785.
30. Beer, A. J., and Schwaiger, M. PET Imaging of αvβ3 Expression in Cancer Patients in Methods in Molecular Biology, Molecular Imaging, Khalid, S., Ed., Springer, **2011**, pp 183-200.
31. Prante, O., Einsiedel, J., Haubner, R., Gmeiner, P., Wester, H.-J., Kuwert, T., and Maschauer S. 3,4,6-Tri-O-acetyl-2-deoxy-2-[18F]fluoroglucopyranosyl Phenylthiosulfonate: A Thiol-Reactive Agent for the Chemoselective 18F-Glycosylation of Peptides. *Bioconjugate Chem.* **2007**, *18*, 254–262.
32. Kuijpers, B. H. M., Groothuys, S., Soede, A. C., Laverman, P., Boerman, O. C., van Delft, F. L., and Rutjes, F. P. J. T. Preparation and evaluation of glycosylated arginine–glycine–asparate (RGD) derivatives for integrin targeting. *Bioconjugate Chem*. **2007**, *18*, 1847-1854.
33. Maschauer, S., Einsiedel, J., Haubner, R., Hocke, C., Ocker, M., Hübner, H., Kuwert, T., Gmeiner, P., and Prante, O. Labeling and Glycosylation of Peptides Using Click Chemistry: A General Approach to 18F-Glycopeptides as Effective Imaging Probes for Positron Emission Tomography. *Angew. Chem. Int. Ed*. **2010**, *49*, 976–979.
34. Collet, C., Maskali, F., Clément, A., Chrétien, F., Poussier, S., Karcher, G., Marie, P.-Y., Chapleur, Y., and Lamandé-Langle, S. Development of 6-[18F]fluoro carbohydrate-based pros-thetic groups and their conjugation to peptides via click chemis-try, *J. Label. Compd. Radiopharm.* **2016**, *59*, 2, 54-62
35. Vala, C., Chrétien, F., Balentova, E., Lamandé-Langle, S., and Chapleur, Y. Neoglycopeptides through direct functionalization of cysteine, *Tetrahedron Lett*. **2011**, *52*, 1, 17-20.
36. Chapleur, Y., Lamandé, S., Collet, C., Chrétien, F. Pro-cess for the preparation of 18F-radiolabeled triazolyl-linked glycopeptides as radiotracers via "click" chemistry, PCT Int., **2014**, WO 2014006022 A1 20140109
37. Pellegrini-Moïse, N., Richard, M., and Chapleur, Y. Exo-glycals as useful tools for anomeric functionalization of sug-ars. In Carbohydrate Chemistry, Rauter, A. P., Lindhorst, T. K., Queneau, Y., Eds, RSC Publishing, **2014**, Vol. 40, 99–117.
38. Richard, M., Didierjean, C., Chapleur, Y., and Pellegrini-Moïse, N. Base- and radical-mediated regio- and stereoselective additions of thiols, thio-sugars and thiol-containing peptides on trisubstituted activated exo-glycals. *Eur. J. Org. Chem*. **2015**, 2632-2645.
39. Tran Thien, H.-T., Novoa, A., Pellegrini-Moïse, N., Chrétien, F., Didierjean, C., and Chapleur, Y. Tetrasubstituted C-Glycosylidenes and C-Glycosyl Compounds from Di- and Mono-bromo-Substituted exo-Glycals. *Eur. J. Org. Chem*. **2011**, 6939–6951.
40. Richard, M., Chateau, A., Jelsch, C., Didierjean, C., Manival, X., Charron, C., Maigret, B., Barberi-Heyob, M., Chapleur, Y., Boura, C., and Pellegrini-Moïse, N. Carbohydrate-based peptidomimetics targeting neuropilin-1: Synthesis, molecular docking study and in vitro biological activities. *Bioorg. Med. Chem*. **2016**, *24*, 5315–5325.
41. Leclerc, E., Pannecoucke, X., Etheve-Quelquejeuc, M., Sollogoub, M. Fluoro-C-glycosides and fluoro-carbasugars, hydrolytically stable and synthetically challenging glycomimetics. *Chem. Soc. Rev*. **2013**, *42*, 4270-4283.
42. Beau, J.-M., Vauzeilles, B., and Skrydstrup, T. C-Glycosyl analogs of oligosaccharides and glycosyl amino acids in Glycoscience. Fraser-Reid, B. O., Tatsuta, K., Thiem, J., Eds, Spring-er, **2001**, Vol. 3, pp. 2679–2724.
43. Li, L., Zhiyuan, Z. Development and Applications of the Copper-Catalyzed Azide-Alkyne Cycloaddition (CuAAC) as a Bioorthogonal Reaction. *Molecules* **2016**, *21*, 10, 1393/1-1393/22.
44. Meyer, J.-P., Adumeau, P., Lewis, J. S., and Zeglis, B. M. Click Chemistry and Radiochemistry: The First 10 Years. *Bioconjugate Chem.* **2016**, *12*, 2791-2807.
45. Bock, V. D., Speijer, D., Hiemstra, H., and van Maarseveen, J. H. 1,2,3-Triazoles as peptide bond isosteres: synthesis and biological evaluation of cyclotetrapeptide mimics. *Org. Biomol. Chem*. **2007**, *5*, 971–975.
46. Lo Conte, M., Pacifico, S., Chambery, A., Marra, A., and Dondoni, A. Photoinduced Addition of Glycosyl Thiols to Alkynyl Peptides: Use of Free-Radical Thiol–Yne Coupling for Post-Translational Double-Glycosylation of Peptides. *J. Org. Chem.* **2010**, *75*, 4644-4647.
47. Petry, N., Vucko, T., Collet, C., Lamandé-Langle, S., Pellegrini-Moïse, N., and Chrétien, F. Synthesis and revised stereo-chemistry assignment of C-allyl glucopyranosides and derivatives. *Carbohydrate Res*. **2017**, 445, 61-64.
48. Han, Z., Achilonu, M. C., Kendrekar, P. S., Joubert, E., Ferreira, D., Bonnet, S. L., and van der Westhuizen, J. H. Concise and scalable synthesis of aspalathin, a powerful plasma sugar-lowering natural product. *J. Nat. Prod*. **2014**, *77*, 583–588.
49. Kulkarni, S. S., and Gervay-Hague, J. Efficient Synthesis of a C-Analogue of the Immunogenic Bacterial Glycolipid BbGL2. *Org. Lett.* **2006**, *8*, 5765–5768.

50. Thota, V. N., Gervay-Hague, J., and Kulkarni, S. S. Synthesis of β-C-galactosyl D- and L-alanines. *Org. Biomol. Chem.* **2012**, *10,* 8132–8139.
51. Lewis, M. D., Cha, J. K., and Kishi, Y. Highly stereose-lective approaches to alpha- and beta-C-glycopyranosides. *J. Am. Chem. Soc.* **1982**, *104*, 4976–4978.
52. Hosomi, A., Sakata, Y., and Sakurai, H. Stereoselective synthesis of 3-(d-glycopyranosyl)propenes by use of allylsilanes. *Carbohydr. Res.* **1987**, *171*, 223–232.
53. Hosomi, A., Sakata, Y., and Sakurai, H. Highly stereoselective c-allylation of glycopyranosides with allylsilanes catalyzed by silyl triflate or iodosilane. *Tetrahedron Lett.* **1984**, *25*, 2383–2386.
54. Martin, A., Salazar, J. A., and Suarez, E. Synthesis of Chiral Spiroacetals from Carbohydrates. *J. Org. Chem.* **1996,** *61*, 3999–4006.
55. Vucko, T., Pellegrini Moïse, N., and Lamandé-Langle, S. Value-added carbohydrate building blocks by regioselective O-alkylation of C-glucosyl compounds, *Carbohydrate Res.* **2019**, *477*, 1-10.
56. Zhang, J., Garriso, J. C., Poluektova, L. Y., Bronich, T. K., and Osna N. A. Livertargeted antiviral peptide nanocomplexes as potential anti-HCV therapeutics. *Biomaterials* **2015**, *70*, 37-47.
57. Miyagawa, A., Tomita, R., Kurimoto, K., and Yamamura H. Selective deprotection of trityl group on carbohydrate by microflow reaction inhibiting migration of acetyl group. *Synth. Commun.* **2016**, *46*, 6, 556–562.
58. Kuhnast, B., and Dollé, F. The challenge of labeling macromolecules with fluorine-18: three decades of research. *Curr. Radiopharm.* **2010**, *3*, 174-201.
59. Humphrey, W., Dalke, A., Schulten, K. VMD: visual molecular dynamics. *Journal of molecular graphics* 1996, *14*, 33-8, 27-8.
60. Xiong, J.P., Stehle, T., Zhang, R., Joachimiak, A., Frech, M., Goodman, S.L., Arnaout, M.A. Crystal structure of the ex-tracellular segment of integrin alpha Vbeta3 in complex with an Arg-Gly-Asp ligand. *Science* **2002**, *296*, 151-155.
61. Gilad, Y., Noy, E., Senderowitz, H., Albeck, A., Firer, M. A., & Gellerman, G. Synthesis, biological studies and molecular dynamics of new anticancer RGD-based peptide conjugates for targeted drug delivery. *Bioorg. Med. Chem.* **2016**, *24*, 294–303.
62. Versteeg, H.H., Heemskerk, J.W.M., Reitsma, P.H. New fundamentals in hemostasis. *Physiol. Rev.* **2013**, *93*, 327–358.
63. Lacolley, P., Regnault, V., Segers, P., Laurent, S. Vascular Smooth Muscle Cell and Arterial Stiffening: Relevance in Development, Ageing and Disease. *Physiol Rev.* **2017**, *97*, 1555–1617.
64. Moiseeva, E.P. Adhesion receptors of vascular smooth muscle cells and their functions. *Cardiovasc Res.* **2001**, *52*, 372-86.

Graphical Abstract

To create your abstract, type over the instructions in the template box below.
Fonts or abstract dimensions should not be changed or altered.

C-glyco"RGD" as $\alpha_{IIb}\beta_3$ and $\alpha_v\beta_3$ integrin ligands for imaging applications: synthesis, in vitro evaluation and molecular modeling

Leave this area blank for abstract info.

Timothé Vucko[a], Nicolas Pétry[a], François Dehez[b], Alexandrine Lambert[b], Antonio Monari[b], Cécile Lakomy[c], Patrick Lacolley[c], Véronique Regnault[c], Charlotte Collet[d,e], Gilles Karcher[d], Nadia Pellegrini-Moïse[a], Sandrine Lamandé-Langle[a,*]

[a]*Université de Lorraine, CNRS, L2CM, F-5400 Nancy, France*
[b]*Université de Lorraine, CNRS, LPCT, F-54000 Nancy, France*
[c]*Université de Lorraine, Inserm, DCAC, F-54500 Nancy, France*
[d] *NancycloTEP, Plateforme d'imagerie moléculaire, F-54511 Vandoeuvre-lès-Nancy, France*
[e] *Université de Lorraine, INSERM, U1254 IADI, F-54000 Nancy, France*